β-decay measurements for $N > 40$ Mn nuclei and inference of collectivity for neutron-rich Fe isotopes

J. M. Daugas,[1] I. Matea,[2] J.-P. Delaroche,[1] M. Pfützner,[3] M. Sawicka,[3] F. Becker,[4] G. Bélier,[1] C. R. Bingham,[5] R. Borcea,[6] E. Bouchez,[7] A. Buta,[6] E. Dragulescu,[6] G. Georgiev,[8] J. Giovinazzo,[9] M. Girod,[1] H. Grawe,[4] R. Grzywacz,[5,10] F. Hammache,[2] F. Ibrahim,[2] M. Lewitowicz,[11] J. Libert,[2] P. Mayet,[4] V. Méot,[1] F. Negoita,[6] F. de Oliveira Santos,[11] O. Perru,[1] O. Roig,[1] K. Rykaczewski,[10] M. G. Saint-Laurent,[11] J. E. Sauvestre,[1] O. Sorlin,[11] M. Stanoiu,[4,6] I. Stefan,[2] Ch. Stodel,[11] Ch. Theisen,[7] D. Verney,[2] and J. Żylicz[3]

[1]*CEA, DAM, DIF, F-91297 Arpajon Cedex, France*

[2]*Institut de Physique Nucléaire, IN2P3-CNRS and Université Paris-Sud, F-91406 Orsay Cedex, France*

[3]*Institute of Experimental Physics, Warsaw University, PL-00681 Warsaw, Hoża 69, Poland*

[4]*Gesellschaft für Schwerionenforschung, D-64291 Darmstadt, Germany*

[5]*Department of Physics and Astronomy, University of Tennessee, Knoxville, Tennessee 37996, USA*

[6]*Horia Hulubei National Institute of Physics and Nuclear Engineering, P.O. Box MG6, Bucharest-Magurele, Romania*

[7]*CEA, Centre de Saclay, IRFU/Service de Physique Nucléaire, F-91191 Gif-sur-Yvette, France*

[8]*CSNSM, UMR 8609, CNRS-IN2P3/Université Paris-Sud, Bâtiment 104, F-91405 Orsay, France*

[9]*Centre d'Etudes Nucléaires de Bordeaux Gradignan, Université Bordeaux I, UMR5797, CNRS/IN2P3, B.P. 120, F-33175 Gradignan, France*

[10]*Physics Division, Oak Ridge National Laboratory, Oak Ridge, Tennessee 37831, USA*

[11]*Grand Accélérateur National d'Ions Lourds, CEA/DSM-CNRS/IN2P3, B.P. 55027, F-14076 Caen Cedex 5, France*

(Received 23 April 2010; revised manuscript received 8 April 2011; published 17 May 2011)

A decay spectroscopic study of the neutron-rich isotopes has been performed using fragmentation of a ^{86}Kr primary beam. Fragments from this reaction have been selected by the LISE2000 spectrometer at the Grand Accélérateur National d'Ions Lourds (GANIL). Half-lives of 29 isotopes, including the first ones identified for ^{61}Ti (15 ± 4 ms), ^{64}V (19 ± 8 ms), and ^{71}Fe (28 ± 5 ms), have been determined and compared with model predictions. ^{67,68}Mn β-delayed γ rays were observed for the first time. The branching for the β-delayed neutron emission was measured to be greater than 10(5)% in the ^{67}Mn decay. The ^{67}Fe isomeric level is firmly determined at higher energy than assigned in previous works. The excitation energies of the first (2^+) and (4^+) states of ^{68}Fe are suggested to lie at 522(1) and 1389(1) keV, respectively, thus bringing confirmation of assignments based on in-beam γ-ray spectroscopy. Beyond-mean-field calculations with the Gogny D1S force have been performed for even-mass nuclei through the Fe isotopic chain. Not only ^{68}Fe but most of the neutron-rich Fe isotopes with neutron numbers below $N = 50$ are interpreted as soft rotors. The calculated mean occupancy of the neutron $g_{9/2}$ and $d_{5/2}$ orbitals in correlated ground states is steadily growing with increasing neutron number throughout the isotopic chain. Interpretation of ^{67}Fe data is based upon the present calculations for the ^{66}Fe and ^{68}Fe even cores.

DOI: 10.1103/PhysRevC.83.054312 PACS number(s): 23.20.Lv, 21.10.Tg, 23.40.−s, 21.60.Jz

I. INTRODUCTION

Dramatic changes in the shell structure are expected for exotic nuclei with very large neutron excess [1–3], featuring erosion of shell gaps and the appearance of new shell closures. Experimental tests of those predictions are challenging, and nuclear spectroscopy studies of neutron-rich exotic nuclei become more and more difficult as the production of such isotopes decreases very quickly with increasing neutron number N.

The $N = 40$ subshell arises from the $l = 3$ harmonic oscillator shell closure. The spin-orbit coupling splits the $l = 4$ g orbital into two configurations; the aligned $g_{9/2}$ is lowered in energy, whereas the antialigned $g_{7/2}$ is increased. As a result, the size of the $N = 40$ gap between the fp shell and the $g_{9/2}$ orbital decreases. The $N = 40$ subshell has been studied in neutron-rich nuclei by several groups theoretically [4–7] and as experimentally [8–13] for many years, as reviewed in [2]. It has been argued that the ^{68}Ni isotope displays a spherical minimum in its potential energy surface and that a second minimum exists near the quadrupole deformation $\beta = 0.3$ corresponding to a 0_2^+ isomeric state [14].

The $\nu g_{9/2}$ orbital is known to play a role in the structure of isotopes with $N < 40$. Along the $N = 35$ isotones, the energy of the first positive-parity state from the $\nu g_{9/2}$ orbital drastically decreases as protons are removed [15]. From ^{63}Ni to ^{59}Cr the position of this orbital goes from 1292 keV down to 503 keV. At $Z = 28$, the spin-isospin components of the central force as well as the tensor force [3] allow a strong attraction between the $\pi f_{7/2}$ and the $\nu f_{5/2}$ orbitals. When protons are removed, this attraction decreases; thus, the energy gap between the νfp and the $\nu g_{9/2}$ orbitals decreases as well. The same effect is observed in the neutron single-particle level diagram calculated for ^{64}Ni [16]. The energy of the 2_1^+ level of the ^{66}Fe$_{40}$ isotope was interpreted as the signature of a well-pronounced prolate deformation with $\beta \approx 0.26$ [9]. More recently, enhanced quadrupole collectivity has been observed in proton inelastic scattering from the $N = 38$ Cr isotope [13]. All this information strongly suggest that the $N = 40$ energy gap is not strong enough to sustain spherical shapes in this mass region and that deformation sets in near $N = 40$. Recent mean-field and beyond-mean-field triaxial calculations [7] show that the $N = 40$ isotones are dynamically deformed

and that their yrast spectroscopy is that of soft rotors for proton number $Z > 20$. Finally, projected shell-model (PSM) calculations point to a soft deformed structure for neutron-rich Fe isotopes in the vicinity of $N = 40$, a picture complementary to that of the deformed shape offered in previous shell-model studies [17].

The present study first reports on β-decay half-life measurements for 29 neutron-rich Ti to Co isotopes [see boxes in red (gray) in Fig. 1], which serves for a critical assessment of model predictions for the $N = 40$ mass region [16]. Measurements of β-delayed γ-ray emission of ^{67,68}Mn that populate ground states and exited levels in the Fe isotopes with $N = 41$ and 42 neutrons are presented. Next, mean-field and beyond-mean-field calculations with the D1S Gogny force [18] are performed to investigate structure properties of even-even Fe isotopes and to assess the role played by neutrons in the vicinity of the $N = 40$ subshell closure. As the collective property of neutron-rich Fe isotopes with $N > 42$ is the topic of current experimental and theoretical interest, these calculations are extended to isotopes with $N \leqslant 50$. Further calculations for $22 \leqslant N \leqslant 40$ are finally performed to map the structure evolution through the $Z = 26$ isotopic chain with the scope of estimating how the neutron $g_{9/2}$ and $d_{5/2}$ orbitals gradually come into play as N increases.

This paper is organized as follows. Section II describes the experimental setup used to measure β-decay half-lives for a number of neutron-rich nuclei in the $A = 60$–70 region. With our experimental setup we have also measured β-delayed γ-ray events for ^{67,68}Mn and identified transitions that form partial level schemes in the daughter ^{67,68}Fe isotopes. An outline of the mean-field and beyond-mean-field methods is provided in Sec. III. The beyond-mean-field method for even-even nuclei consists of mixing configurations in the framework of the generator coordinate method (GCM) treated using the Gaussian overlap approximation (GOA). As a result, physical states with parity $\pi = +$ are calculated for even-A Fe isotopes solving a quadrupole collective Hamiltonian in five dimensions (5DCH). Next, Sec. IV discusses the present predictions for low-lying levels with angular momentum $I \leqslant 6$ and comparisons with experimental data. As the collective picture stemming from our calculations is close to that provided in Ref. [17], we briefly discuss why both models lead to similar conclusions. Next, complementary calculations are presented that are performed to estimate the mean occupancies of the $\nu g_{9/2}$ and $\nu d_{5/2}$ neutron orbitals and to delineate their evolution throughout the isotopic chain. Finally, the low-lying level scheme measured for ^{67}Fe is interpreted by means of our calculations for ^{66}Fe and ^{68}Fe. Spin and parity assignments are tentatively made, and isomeric state properties are discussed.

II. EXPERIMENTAL SETUP AND RESULTS

The experiment has been performed at the Grand Accélérateur National d'Ions Lourds (GANIL) using the LISE2000 spectrometer [19]. The neutron-rich ^{86}Kr beam with an energy of 57.8 MeV per nucleon and an average intensity of approximately 3 μAe impinged on a rotating 50-mg/cm^2-thick ^{nat}Ta target tilted at 30°. A 23-mg/cm^2-thick carbon foil placed behind the target allowed a reduction of the charge states distribution width of the produced fragments, yielding mainly fully stripped ions with a few percent of charge $Q = Z - 1$. A 220-μm-thick beryllium wedge was used in the first dispersive plane of the spectrometer to remove light fragments and further suppress ions that were not fully stripped. The average time of flight of the reaction products was about 200 ns because the detector setup was mounted at the achromatic focal point of the LISE2000 spectrometer only 19 m away from the target. The heavy ions were detected by a three-element Si-detector telescope with thicknesses of 300 μm, 300 μm, and 1 mm, respectively. Selected ions were stopped in the last Si detector, a double-sided silicon-strip detector (DSSSD) with 16×16 strips of 3-mm pitch. The DSSSD was backed by a 3.5-mm-thick Si(Li) detector acting as a veto counter for transmitted ions and β particles. The Si telescope was surrounded by four clover-type EXOGAM germanium detectors. The total photopeak efficiency measured with calibration sources was found to be 5.5(5)% at 1.33 MeV and 26(4)% at best for a γ-ray energy of about 120 keV. The

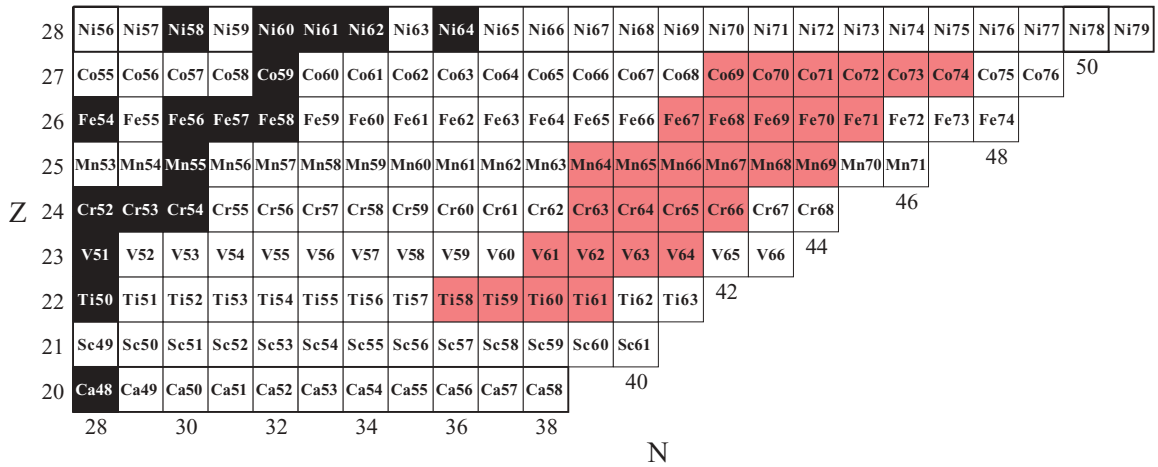

FIG. 1. (Color online) The region of the chart of the nuclides identified as bound from doubly magic ^{48}Ca to ^{79}Ni. Stable nuclides are shown in black and those presently produced are highlighted in red (gray).

DSSSD detector also served as a β detector. The β detection efficiency was determined using the decay of ^{78}Ga [20] and was found to be approximately 20%.

The fragment reaction products were identified in mass A, atomic number Z, and charge Q by measuring their energy loss in the Si telescope and their time of flight in the spectrometer [21]. During the experiment, an average of 0.6 ions per second was implanted into the DSSSD detector, giving a maximum implantation of 0.16 ions per second in the most frequently hit strip. Thus, an average time between two implantations is much longer than the average β-decay lifetime, usually of the order of a few hundreds of milliseconds for the nuclei of interest, allowing for time correlation between the implanted ion and the β decay. The granularity of the strip detector provided a clean spatial correlation between the implanted ion and its detected β decay. The average rate of the β particles correlated with a γ ray was about 20 per second. The β background events were mainly originating from the decay of long-lived nuclei populated by the chain of decays of implanted nuclei in the DSSSD detector. The half-lives of nuclei have been determined by setting a 3-s time correlation between ions implanted in the strip (x_i, y_i) and β signals in the same strip. During this period, not only the decay of the selected nucleus but also those of its daughter and granddaughter could be recorded. Thus, the fitting procedure to determine β-decay half-lives includes five free parameters as described in [22], namely, the β-detection efficiency, background rate, and mother, daughter, and granddaughter half-lives. A χ^2 minimization was used for nuclei observed with more than 400 β correlation events, whereas the likelihood normalization method is used for lower correlation yields. For very neutron-rich nuclei a strong β-delayed neutron branch is expected [23]. This branch for Co and Ni isotopes is of the order of 10% [24]. The β-delayed neutron probability was not taken into account in the present fitting procedure. Half-lives of the daughter and granddaughter were taken as free parameters. As a result, both parameters implicitly depend upon the β-delayed neutron branch. The deduced β-detection efficiencies were found to be similar for all nuclei, which means that the fitting procedure presently used is reliable. The β-delayed γ-ray correlation was obtained by recording all β-γ events coincident within 10 μs. The β-delayed γ rays from the decay of $^{70-73}$Co to $^{70-73}$Ni observed in the present experiment were reported in Refs. [25,26].

Results of β-decay half-lives of the isotopes produced in this experiment are discussed in Sec. II A. Sections II B and II C focus on results for the β-decay properties of ^{67,68}Mn isotopes, respectively. In total, 3535 ions of ^{67}Mn and 722 ions of ^{68}Mn have been implanted into the DSSSD detector. Possible spin and parity assignments to the mother nuclei and low-lying excited states of the daughter nuclei ^{67,68}Fe are discussed in Secs. II B2 and II C. The low production rate of ^{69}Mn (100 ions) did not allow for the observation of any β-γ correlation.

A. Half-life measurements

Many reaction products were observed in this experiment. Their β-decay half-lives are gathered in Table I. The ^{61}Ti, ^{64}V, and ^{71}Fe half-lives are presented here. The decay patterns of these isotopes are shown in Figs. 2(a), 2(b), and 2(c), respectively. Other half-lives determined in the present work are in good agreement with those reported in previous publications [9,22,24,27–34]. Those quoted by Ameil *et al.* [35] are not considered as reported values since they are impaired by systematic errors [9,28,36].

Discrepancies between the present and previous measurements occur in some cases, for example, ^{66}Cr and ^{71}Co [22,27]. One reason could be that the daughter and granddaughter half-lives of both nuclei were taken as fixed parameters in

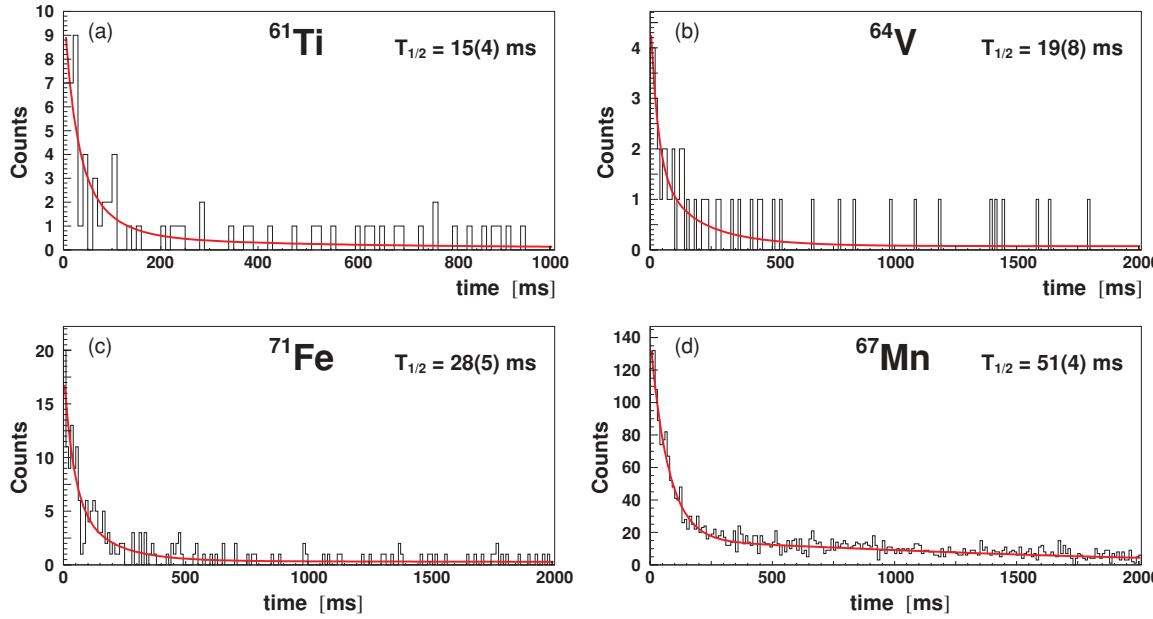

FIG. 2. (Color online) β-decay curves of ^{61}Ti (a), ^{64}V (b), ^{71}Fe (c), and ^{67}Mn (d). The corresponding half-lives $T_{1/2}$ are shown for each nuclide.

TABLE I. β-decay half-lives $T_{1/2}$ for the neutron-rich Ti, V, Cr, Mn, Fe, and Co isotopes measured in the present work compared with previous measurements. Calculations are from Ref. [16].

Nucleus	This work	$T_{1/2}$ (ms) Previous works	Calculations
^{58}Ti	57(10)	59(9) [22], 47(10) [28]	152.3
^{59}Ti	27.5(25)	30(3) [22], 58(17) [28]	21.3
^{60}Ti	22.4(25)	22(2) [22]	53.6
^{61}Ti	15(4)		27.6
^{61}V	52.6(42)	43(7) [28], 47.0(12) [29]	26.9
^{62}V	33.6(23)	65(31) [28], 33.5(20) [29]	20.8
^{63}V	19.2(24)	17(3) [29]	17.8
^{64}V	19(8)		8.3
^{63}Cr	128(8)	129(2) [22], 113(16) [28]	96.6
^{64}Cr	42(2)	43(1) [22], 44(12) [28]	153.9
^{65}Cr	28(3)	27(3) [22]	100.6
^{66}Cr	23(4)	10(6) [22]	71.0
^{64}Mn	90(9)	89(4) [9], 91(4) [27], 85(5) [28]	41.5
^{65}Mn	84(8)	88(4) [9], 92(1) [27], 100(8) [28]	28.9
^{66}Mn	65(5)	66(4) [9], 64(2) [27], 62(14) [28]	23.1
^{67}Mn	51(4)	42(4) [9], 47(4) [27]	25.0
^{68}Mn	29(4)	28(4) [9], 28(8) [27]	14.1
^{69}Mn	18(4)	14(4) [9]	14.1
^{67}Fe	304(81)	394(9) [27], 500(100) [28], 416(29) [30]	1138.9
^{68}Fe	180(19)	187(6) [27], 155(60) [28], 100(60) [31]	767.3
^{69}Fe	110(6)	109(9) [27]	402.1
^{70}Fe	71(10)	94(17) [27]	245.3
^{71}Fe	28(5)		117.5
^{69}Co	229(24)	232(17) [27], 270(50) [31], 220(20) [32]	76.6
^{70}Co	108(7)	121(8) [27], 92(25) [28], 120(30) [33]	47.5
^{71}Co	79(5)	97(2) [27]	39.4
^{72}Co	62(3)	59(2) [34]	31.6
^{73}Co	41(4)	41(6) [24]	25.6
^{74}Co	19(7)	30(3) [34], 34^{+6}_{-9} [24]	18.7

Refs. [22,27]. We also note that the ^{60}Ti, ^{68}Fe, and ^{70}Fe half-lives were determined assuming the daughter half-lives as free parameters [22,27]. Except for the ^{70}Fe nucleus, these former mother half-lives agree with the present values. The discrepancy noted between the values taken by the ^{70}Fe half-life in previous and present experiments may stem from counting statistics, which here are found to be four times higher than those reported in Ref. [27]. Moving to ^{74}Co, the present half-life is much shorter than that deduced from fragmentation reactions [24,34]. There, statistics were more than a factor of two higher than in present measurements, which could explain the observed discrepancy. One can note that the half-lives of the ^{72,73}Co isotopes are in very good agreement with previous experiments [24,34].

The experimental values shown in Table I are now compared with predictions based on quasiparticle random phase approximation (QRPA) and the finite-range droplet model (FRDM) calculations [16,37]. The predictions shown in Table I are underestimating (overestimating) the odd-Z (even-Z) measurements. These differences are interpreted as stemming from adopted quadrupole deformations, which are not appropriate to the β-decay precursors. Other model calculations based on the extended Thomas-Fermi plus Strutinsky integral (ETFSI) seem to provide more realistic estimates for deformations. For example, the ETFSI calculations indicate strong prolate quadrupole deformations ($\beta > 0.2$) for neutron-rich Cr and Fe isotopes. Deformations from FRDM and ETFSI calculations are close for ^{63}Cr (i.e., $\beta = 0.33$ and $\beta = 0.31$ from [37] and [38], respectively), and estimates for the β-decay half-life are within 30% of the experimental value. For other Cr and Fe the ratio between experimental and calculated half-life values is far from unity. These comments are intended to illustrate the point that such structure models in which axial symmetry is assumed generally fail to provide reliable half-life estimates for the neutron-rich nuclei of present concern. It would be interesting to challenge the present data with predictions from a model including triaxial deformations [39], which are typical to this mass region; see Sec. III.

B. ^{67}Mn decay

1. *Half-life and β-γ coincidences*

The ^{67}Mn β-decay pattern is presented in Fig. 2(d). A half-life of 51(4) ms has been determined for the ^{67}Mn ground state. A mean average value of 47(4) ms is adopted according to the previous measurements of 42(4) ms [9] and 47(4) ms [27].

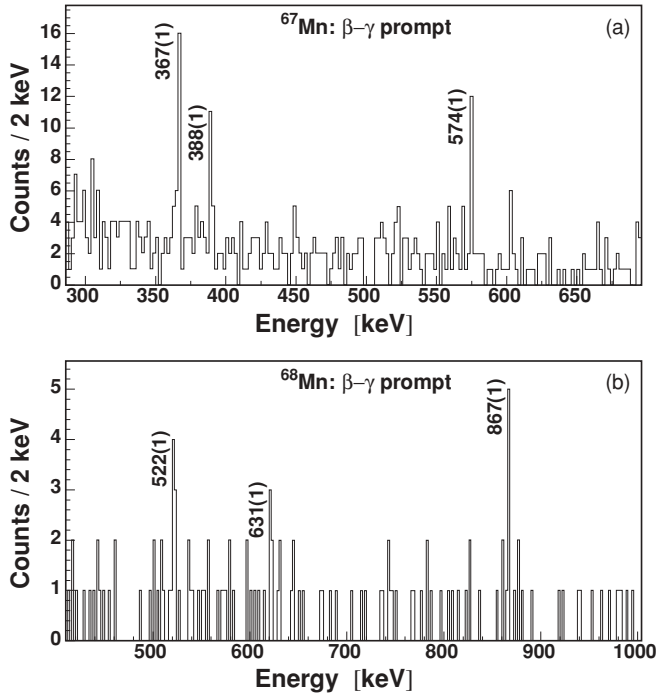

FIG. 3. Prompt β-γ spectra of (top) ^{67}Mn and (bottom) ^{68}Mn from the present measurements.

The prompt β-γ decay spectrum of ^{67}Mn shown in Fig. 3(a) leads to the identification of γ lines with energies of 367(1) and 388(1) keV. These energies are consistent with previous results for the decay of the isomeric state of ^{67}Fe [15,40,41], namely, 366.4(5) and 387.7(5) keV. A 574(1)-keV γ-ray energy has also been observed in the prompt β-γ decay of ^{67}Mn. This γ ray is associated with the $2_1^+ \rightarrow 0_1^+$ transition in ^{66}Fe arising from the β-delayed neutron decay, estimated to occur with a lower limit probability of 10(5)%, deduced from the observed γ-ray intensity of the $2_1^+ \rightarrow 0_1^+$ transition in ^{66}Fe. This result is consistent with recent dedicated measurements for Co and Ni nuclides [24].

2. ^{67}Fe level scheme

The structure of ^{67}Fe has been the topic of many discussions [15,40] at a time when only isomeric transitions were identified. The present ^{67}Mn β decay and β-γ coincidence data provide new information on the energies and spin and parity assignments for the levels fed by the ^{67m}Fe decay, as discussed below. A review of previous works is first made, which here serves to settle on firmer ground the spins and parities of low-lying levels, including the isomeric level.

The first time the isomer was observed it was thought that its decay proceeds through a single delayed 367-keV $M2$ transition between $\nu g_{9/2}$ and $\nu f_{5/2}$ single-particle spherical states [15]; see Fig. 4(a). This interpretation was proved wrong by later experiments devoted to the study of microsecond isomeric states in this region [40,41], where two independent experiments revealed that this isomer decays via two γ-ray transitions of 366.4(5)- and 387.7(5)-keV energies, with an intensity ratio $I_\gamma(387.7)/I_\gamma(366.4) = 0.11(2)$. Thus, the energy of the isomeric state was suggested to equal 388 keV, implying that the 367-keV γ ray is emitted in a cascade including a nonobserved highly converted 20-keV transition; see Fig. 4(b). A mean average half-life of 64(14) μs was adopted [41].

In the present experiment the two γ lines are observed in prompt β-γ correlation, suggesting that the 388-keV level is not isomeric. The isomer then should be located at an excitation energy above 388 keV, which decays through a highly converted transition and/or γ-ray emission with too low an energy to be observed; see Fig. 4(c). No delayed γ ray has been observed following the β decay of ^{67}Mn, which means that the ^{67m}Fe is not fed or that the feeding is below the level at which it could be measured in the current experiment. The β-decay intensity ratio between the two observed γ rays is found to be $I_\gamma(388)/I_\gamma(367) = 0.77(26)$ after being corrected for detection efficiencies. The differences between the γ intensity ratios in β decay and the isomeric decay imply that these transitions originate from two different initial states located at 366.4(5) and 387.7(5) keV feeding the ground state. No information concerning the direct feeding of these states and the ground state by the ^{67}Mn β decay could be extracted from the present data.

We now proceed to spin and parity assignments. In a recent Penning trap experiment [42], a long-lived $T_{1/2} = 1.12(15)$ s [30] isomer has been identified in ^{65}Fe at 402(5)-keV excitation energy, which, from systematics, has been assigned $I^\pi = (9/2^+)$. This suggests an assignment originating from the $\nu g_{9/2}$ orbital for ^{67m}Fe, namely, $I^\pi = (1/2 - 9/2)^+$, assuming deformation. This implies revision of the previously suggested decay modes and assignments [40] for states below the isomer. No evidence is found for the existence of a transition between the 387.7(5)- and 366.4(5)-keV levels. The ground state of ^{67}Fe has recently been assigned as $I^\pi = (1/2^-)$ [30]. Taking into account these assignments and the β decay of ^{67}Mn, the two excited states in ^{67}Fe should have negative parities. As the systematics suggest $I^\pi = (5/2^-)$ for the ^{67}Mn ground state, the allowed β decay would feed $I^\pi = (3/2, 5/2, 7/2)^-$ states. The $I^\pi = 7/2^-$ state arises from the coupling of a single-particle proton state with the even-A core 2^+ state. The energy of the 2^+ state for ^{66}Fe is 574 keV, higher than the observed states in ^{67}Fe. The systematics on the $^{58-61}$Fe isotopes show that the energy of the $7/2^-$ state is about 150 keV higher than those for the neighboring 2^+ states. Moreover, the feeding of the $7/2^-$ states following the β decay of odd-mass Mn isotopes is lower than 1%. Thus, a spin $7/2^-$ might be excluded, and $I^\pi = (3/2, 5/2)^-$ could be assigned to the 366.4(5)- and 387.7(5)-keV states. Since no transition was observed between the isomeric and ground states, we can exclude the assignments $I^\pi = 1/2^+$ and $3/2^+$ for the isomer. On the other hand, according to the low-energy transition and the half-life of the isomer, the multipolarity of the isomeric transition should be $L = 1$, which excludes the assignments $I^\pi = 9/2^+$. For a nonobserved transition below 30 keV, the energy limitation of our setup, only $E1$ transitions to $(3/2^-, 5/2^-)$ levels lead to half-lives compatible with that measured. A $M2$ (or $E3$) branch from the isomer to the ground state will be suppressed by the l forbiddance of such intrinsically $\nu g_{9/2} \rightarrow \nu p_{1/2}$ transition. There is no reason to exclude either $I^\pi = 5/2^+$ or $I^\pi = 7/2^+$

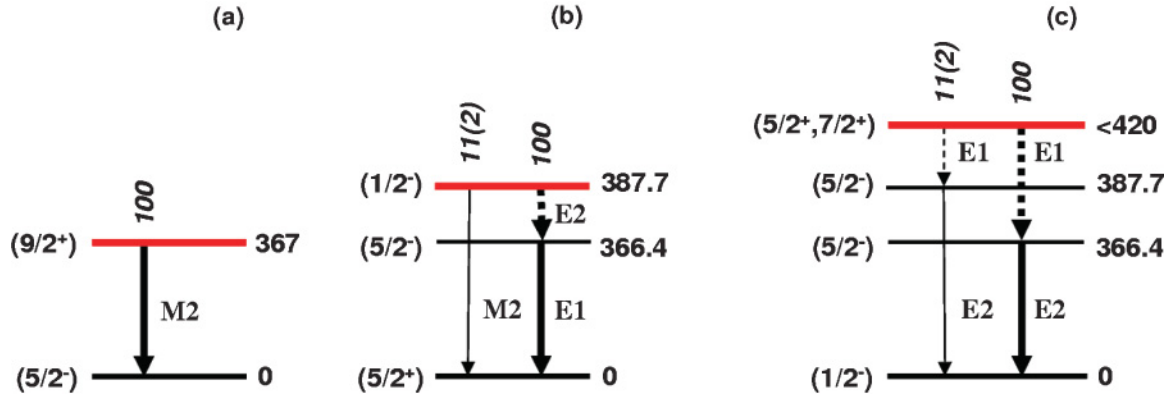

FIG. 4. (Color online) ^{67m}Fe decay schemes from (a) Ref. [15], (b) Refs. [40,41], and (c) the present measurements. Tentative spin and parity assignments in (c) are based on calculations discussed in Sec. IV B. The dashed line is for nonobserved transition. The red (gray) line is for the isomeric level.

for the spin and parity assignments to the isomeric level. The present assignments are summarized as follows: $(1/2^-)$ (ground state), $(3/2^-, 5/2^-)$ (366.4 keV), $(3/2^-, 5/2^-)$ (387.7 keV), $(5/2^+, 7/2^+)$ (isomer). Figure 5(a) shows the β decay of ^{67}Mn together with the presently observed γ rays and spin and parity assignments. Assignments based on present mean-field calculations will be discussed in Sec. IV B.

C. ^{68}Mn decay

A half-life of 29(4) ms has been extracted for the ^{68}Mn ground state. A weighted mean average value of 28.4(27) ms is adopted using the previous measurements of 28(4) ms [9] and 28(8) ms [27]. The prompt β-γ spectrum of ^{68}Mn is shown in Fig. 3(b), revealing three γ-line energies of 522(1), 631(1), and 867(1) keV. The 631(1)-keV transition arises from the β decay of ^{68}Fe to ^{68}Co. The two others are tentatively assigned, according to the systematics and to the β decay of even-mass Mn isotopes [9], to the $2_1^+ \rightarrow 0_1^+$ (522 keV) and $4_1^+ \rightarrow 2_1^+$ (867 keV) transitions in ^{68}Fe, respectively [41]. These γ-ray energies are in good agreement with those recently observed by Adrich *et al.* [43] and are tentatively assigned as above. However, the accuracy achieved in energy determination is here superior to that obtained previously with in-beam γ-ray spectroscopy.

Intensities observed in Fig. 3 for the 522- and 867-keV transitions are similar. This implies that the ^{68}Mn β decay feeds excited states lying above the (4_1^+), $E_x = 1389$ keV level in ^{68}Fe. This suggests that the β-decay level in ^{68}Mn has spin $I > 3$, as indicated in Fig. 5(b).

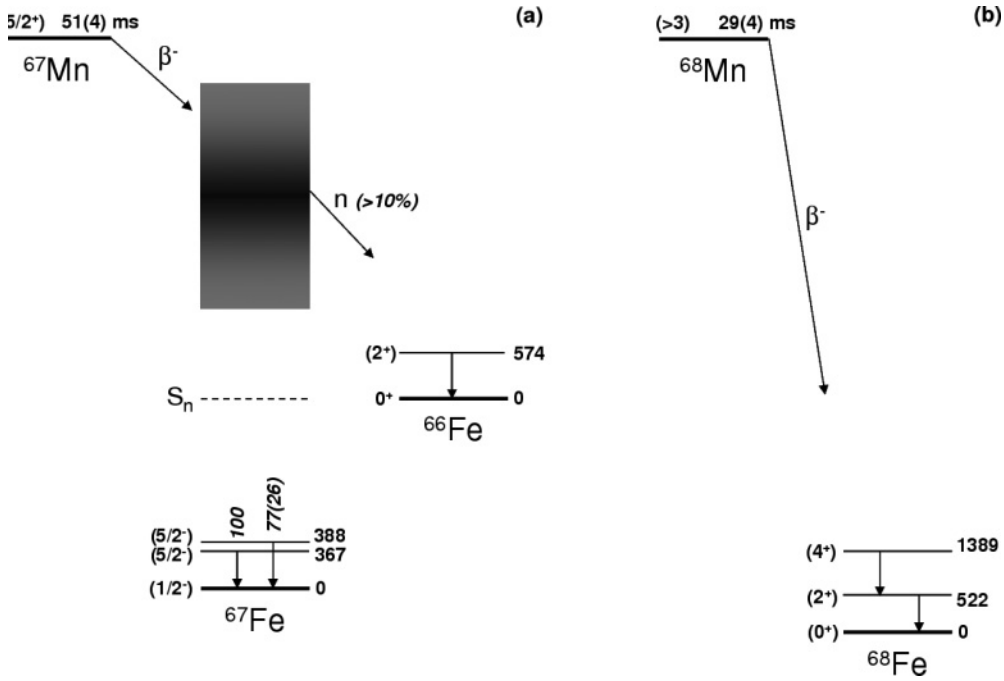

FIG. 5. Decay of the (a) ^{67}Mn and (b) ^{68}Mn nuclei with spin and parity assignments inferred from the present experiment.

III. MEAN-FIELD AND BEYOND-MEAN-FIELD CALCULATIONS

The parity $\pi = +$ low-lying collective levels of even-mass Fe nuclei were calculated with a microscopic collective model in five dimensions using the D1S Gogny force, as described and implemented in Refs. [44,45]. For the specific purpose of the present study, we indicate that (i) the constrained Hartree-Fock-Bogoliubov (HFB) equations were solved by expending the single-particle states onto a triaxial harmonic oscillator basis including 11 major shells and (ii) the collective masses entering the 5DCH Hamiltonian were renormalized to fulfill their relationships with the Thouless-Valatin-like moment of inertia [45,46] along symmetry axes [47]. No effective charge was involved in the calculations.

IV. INTERPRETATIONS

A. Even-even nuclei

1. Level schemes

The mean-field and beyond-mean-field calculations for the isotopes ^{66}Fe and ^{68}Fe adjacent to ^{67}Fe are shown in Fig. 6. The right panels show the potential energies calculated over the (β,γ) plane, where the stars mark the location of calculated 0^+ ground states as specified by their mean $\langle\beta\rangle_{0^+}$ and $\langle\gamma\rangle_{0^+}$ deformations. The left panels show, for illustration purposes, the $I \leqslant 6\hbar$ yrast levels on an energy scale defined with respect to the bottom of the potential energy surface, here reduced to axial symmetry. Both ^{66}Fe and ^{68}Fe isotopes are spherical at the mean-field level and become deformed in the beyond-mean-field calculations. In the left panels of Fig. 6, the horizontal bars are centered on the mean values of the axial deformations at the given spin. For ground states, these mean values are $\langle\beta\rangle_{0^+} = 0.261$ (^{66}Fe) and $\langle\beta\rangle_{0^+} = 0.254$ (^{68}Fe). It turns out that both nuclei are also triaxial with $\langle\gamma\rangle_{0^+} \approx 20^\circ$ (for the definition of mean deformations, see Ref. [44]). These features are consistent with the topology of the ^{66,68}Fe potential energy surfaces, which show that these isotopes are soft against axial and triaxial quadrupole deformations. This interpretation is also supported by the calculated mean deformation $\langle\beta\rangle$, which displays a strong increase through yrast bands. $\langle\beta\rangle$ takes on values from $\langle\beta\rangle_{0^+} = 0.261$ (0.254) to $\langle\beta\rangle_{6^+} = 0.394$ (0.368) for ^{66}Fe (^{68}Fe) with increasing angular momentum. Over six units of angular momentum, the kinematic moments of inertia increase sharply from $\mathcal{J}^{(1)} = 3.86$ (3.90) to $\mathcal{J}^{(1)} = 8.93$ (8.56) $\hbar^2$ MeV^{-1} for ^{66}Fe (^{68}Fe). As our microscopic model is adiabatic in nature, the spectacular stretching calculated for these deformed nuclei as angular momentum increases is interpreted as a consequence of their softness against deformation. The experimental values of the kinematic moments of inertia are higher than those calculated but show the same trend going from $\mathcal{J}^{(1)} = 5.23$ (5.75) to $\mathcal{J}^{(1)} = 8.33$ (8.07) $\hbar^2$ MeV^{-1} for ^{66}Fe (^{68}Fe) at angular momenta up to $I = 4$. Even though these isotopes are deformed, their yrast spectra do not display clear-cut rotational level sequences. ^{66}Fe and ^{68}Fe are stretching significantly as angular momentum increases, which leads to dramatic distortion of their rotational spectra.

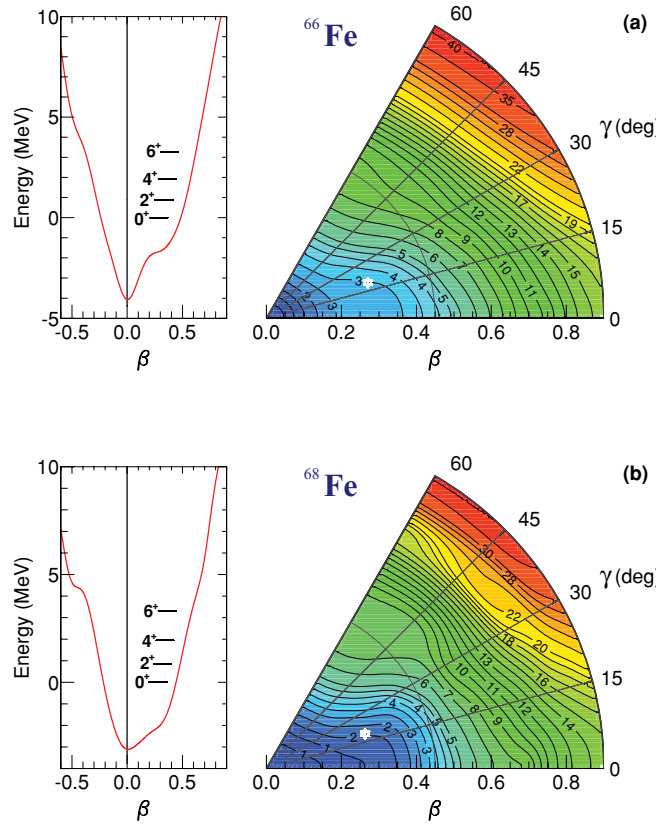

FIG. 6. (Color online) Mean-field and beyond-mean-field calculations for (a) ^{66}Fe and (b) ^{68}Fe. The right panels show the potential energy surfaces including ZPE corrections. The location of the ground state with mean $\langle\beta\rangle_{0^+}$ and $\langle\gamma\rangle_{0^+}$ deformations is marked with a star. The solid curves in the left panels are for the potential energies along the axial symmetry axis. Energies of the $I \leqslant 6\hbar$ yrast levels are shown as horizontal bars centered on the mean axial quadrupole deformations calculated as explained in the text.

To get more insights into the structure of neutron-rich Fe isotopes, a comparison is made between experimental and calculated 2_1^+ energies. To enlarge the scope, this comparison covers neutron numbers from $N = 24$ to $N = 50$, as shown in Fig. 7. Except for the isotope at the $N = 28$ shell closure, the experimental 2_1^+ energies display near-constant values around 0.8 MeV for $N \leqslant 36$ and a smooth decrease beyond this neutron number. The overall pattern of the calculated 2_1^+ energies is similar to that for experimental values. However, the calculated energies are about 300 keV higher for $N \geqslant 30$, a feature rather common to the 5DCH calculations [45]. Using the D1M effective force instead of the D1S effective force [48] in the 5DCH calculations for Fe isotopes does not help reduce the energy differences. The D1S calculations also show that the 2_1^+ energies slightly decrease beyond $N = 42$ until $N = 48$ is reached, the neutron number that marks the upper limit for the deformation region spanned by the neutron-rich Fe isotopes.

The energy ratio $R_{42} = E(4_1^+)/E(2_1^+)$ usually serves as a structure indicator [49], with $R_{42} = 2.0$ and $R_{42} = 3.3$ for

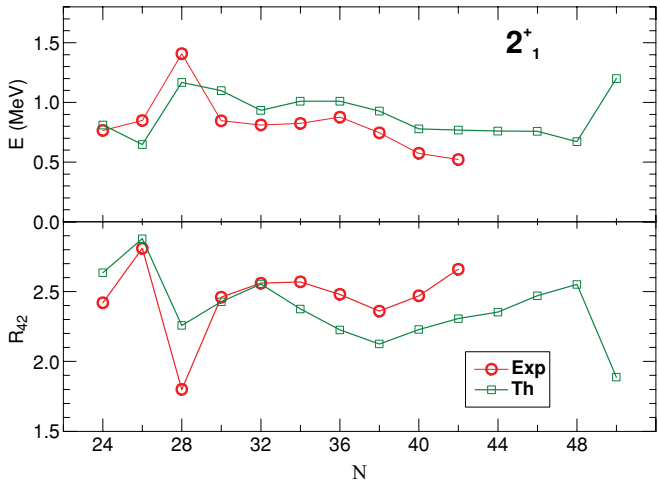

FIG. 7. (Color online) (top) Experimental (open circles) and calculated (open squares) excitation energies of the first 2^+ level in the even-mass Fe isotopic chain. (bottom) Experimental and calculated values of the energy ratio R_{42} between yrast 4^+ and 2^+ levels.

harmonic vibrators and axial rotors, respectively. One can note in Fig. 7 that the calculated ^{76}Fe spectrum is characterized by a ratio R_{42} smaller than 2.0. This originates from anharmonic features in the potential energy surface. Both experimental and calculated R_{42} values shown in Fig. 7 display (i) values that are intermediate between these limits for all the neutron-rich Fe isotopes except ^{76}Fe and (ii) a clear-cut minimum at the neutron midshell$N = 38$. Most neutron-rich Fe isotopes may be viewed as soft rotors with negative spectroscopic quadrupole moments $Q(I^\pi)$, $I^\pi = 2_1^+, 4_1^+$, and 6_1^+, suggesting prolate shapes.

2. 5DCH versus PSM

It is gratifying that this conclusion matches that in Ref. [17], where another microscopic model description based on a projected shell model was employed. Actually, the two models rely upon different physical pictures. On the one hand, PSM assumes (i) axial symmetry, and (ii) a multiparticle-multihole energy functional at fixed quadrupole deformation. On the other hand, 5DCH assumes (i) triaxial symmetry and (ii) a HFB quasiparticle vacuum over β and γ deformations as an energy functional. These are the elementary building blocks specific to each model. Restoration of angular momentum in the PSM is performed using standard techniques, while this is accomplished in 5DCH through resorting to the GCM + GOA approach. Furthermore, the 5DCH model is adiabatic in nature, while PSM is not. Finally, the conclusions reached separately in the model studies, that neutron-rich Fe isotopes behave as soft rotors at low spin and excitation energy, are rooted in (i) rotational alignment in PSM and (ii) softness of the potential energy against quadrupole deformations in 5DCH. A subtle difference, however, exists between both interpretations. With PSM, nuclei are interpreted as soft rotors against axial deformation, while nuclei are soft rotors against both axial and triaxial deformations in 5DCH. Indeed, predictions of the models at high spin will deviate from each other, as they should.

3. Orbital occupancies

Further insights into structure properties are provided by the occupation number of neutron and proton orbitals. Here we focus on correlated ground states from the beyond-mean-field calculations and first evaluate the $\pi f_{7/2}$ and $\nu g_{9/2}$ occupation numbers at deformation $\beta = \langle\beta\rangle_{0^+}$ from constrained HFB calculations performed while enforcing axial symmetry. Obviously, this method is crude since, for example, it ignores the dependence of correlated ground states upon the γ degree of freedom. However, this may not be a major concern here as recent mean-field studies based on a Gogny force have concluded that occupancies are more sensitive to the magnitude of axial deformation than to γ deformation [50]. We therefore view the present occupation numbers as reasonable estimates.

The occupation numbers n_j calculated for the $\pi f_{7/2}$ and $\pi p_{3/2}$ proton orbitals through the isotopic chain are nearly constant, with $n_{f_{7/2}} \approx 5.8$ and $n_{p_{3/2}} \approx 0.15$. These values deviate from those expected ($n_{f_{7/2}} = 6$ and $n_{p_{3/2}} = 0$) from the independent particle model. The depletion of the $\pi f_{7/2}$ orbital and, conversely, the nonzero occupancy of the $\pi p_{3/2}$ orbital arise both from short-range correlations tied to the pairing field and from the long-range correlations treated in our beyond-mean-field approach. The structure evolution along the Fe isotopic chain appears mostly tied to the variation of neutron level occupancies, the values of which are also governed by short- and long-range correlations.

The occupation numbers calculated for $\nu g_{9/2}$ orbitals are shown as open squares in Fig. 8, where they display very weak values for $N \leqslant 30$ and a steady increase for higher neutron numbers. These results are consistent with suggestions that the $N = 40$ subshell gap in the Ni region is weakening already for $N > 34$ and possibly at $N = 32$ [29,51–54]. A few $g_{9/2}$ orbital occupancies have been reported previously. These are based on axially symmetric HFB calculations with the SkM* force ($N = 38, 40$) [55] and the shell-model Monte Carlo approach in which the full fp-gds valence space is considered ($N = 32, 36, 40$) [56]. Shown as solid squares and triangles in Fig. 8,

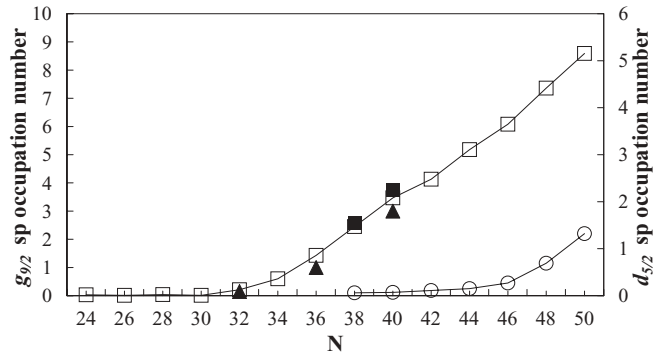

FIG. 8. Present occupation number estimates for the neutron $g_{9/2}$ (open squares) and $d_{5/2}$ (open circles) orbitals along the even-mass Fe isotopic chain. The lines are to guide the eye. Solid triangles are average $g_{9/2}$ occupation numbers from shell-model Monte Carlo calculations in the complete fp-gds valence space [56], and solid squares are $g_{9/2}$ occupation numbers from mean-field HFB calculations with the SkM* force [55].

these occupancies take on a smooth increase with increasing N. Similar calculations have also been performed presently for the $\nu d_{5/2}$ orbital. Its occupation number increases more gradually than that for the $\nu g_{9/2}$ orbital, and it remains small (see open circles in Fig. 8).

These conclusions are of broad relevance, particularly for the neutron-rich Cr isotopes as emphasized in a recent paper [13], and they are consistent with shell-model calculations [17,29,51]. Our calculated occupancies for proton and neutron orbitals, governed by the D1S shell gaps, are to be contrasted with results from recent shell-model calculations in which the valence space has been considerably expanded for the neutron-rich Fe region [57,58]. Such calculations indicate that the $Z = 28$ shell gap is reduced as the neutron $g_{9/2}$ shell gets filled and that this gap decreases for $Z < 28$.

B. The even-odd ^{67}Fe nucleus

To get more insight into the ^{67}Fe level scheme, we base our model analysis on neutron single-particle (sp) levels calculated assuming axial symmetry in HFB calculations. As ^{66}Fe and ^{68}Fe form the even cores of ^{67}Fe, neutron sp levels are shown as functions of the deformation for both isotopes in Fig. 9. The starting point of the analysis consists of selecting which deformation would be appropriate. In the following, we present two different coupling scenarios, namely, the particle-plus-rotor and rotation-alignment schemes.

1. *Particle-plus-rotor scheme*

We first make the choice of fixing the ^{67}Fe ground-state deformation at the mean deformation $\langle\beta\rangle_{0^+}$ previously established for ^{66}Fe and ^{68}Fe, that is, $\beta(^{67}\text{Fe}) = 0.261$ and $\beta(^{67}\text{Fe}) = 0.254$, respectively. At either deformation, marked as a vertical line in Figs. 9(a) and 9(b), the ground state (gs) is identified as a $K^\pi = 1/2^-$ level originating from the $\nu p_{1/2}$ orbital. The decoupled rotational band built upon the gs requires knowledge of the decoupling parameters a and moments of inertia $\mathcal{J}_x$, where the energy is

$$E_{rot}(I^\pi) = \hbar^2/2\mathcal{J}_x[I(I+1) - K^2 + a(-)^{I+1/2}(I+1/2)],$$

assuming that K is the projection of angular momentum I on the z axis. The parameters a and $\mathcal{J}_x$ are next determined in new HFB calculations in which one neutron quasiparticle (qp) state is blocked at $\beta(^{67}\text{Fe}) = 0.261$ and $\beta(^{67}\text{Fe}) = 0.254$ deformations. The decoupling parameter a takes on values of -0.9266 and -0.9349, respectively. The moments of inertia are calculated using the Inglis-Belyaev formula [59,60]. As this formula was designed for even-even nuclei, the actual $\mathcal{J}_x$ calculations for ^{67}Fe were performed while requiring that the blocked qp level does not contribute. The calculated reciprocal moments of inertia $\hbar^2/2\mathcal{J}_x$ have values of 31.1427 and 29.9543 keV, respectively, for the two deformations. Decoupled rotational bands are shown in the left and middle panels of Fig. 10 for the two even-core mean deformations up to spin $I^\pi = 11/2^-$. The ground-state spin is found to be $I^\pi = 1/2^-$, just few keV below the band member $I^\pi = 3/2^-$.

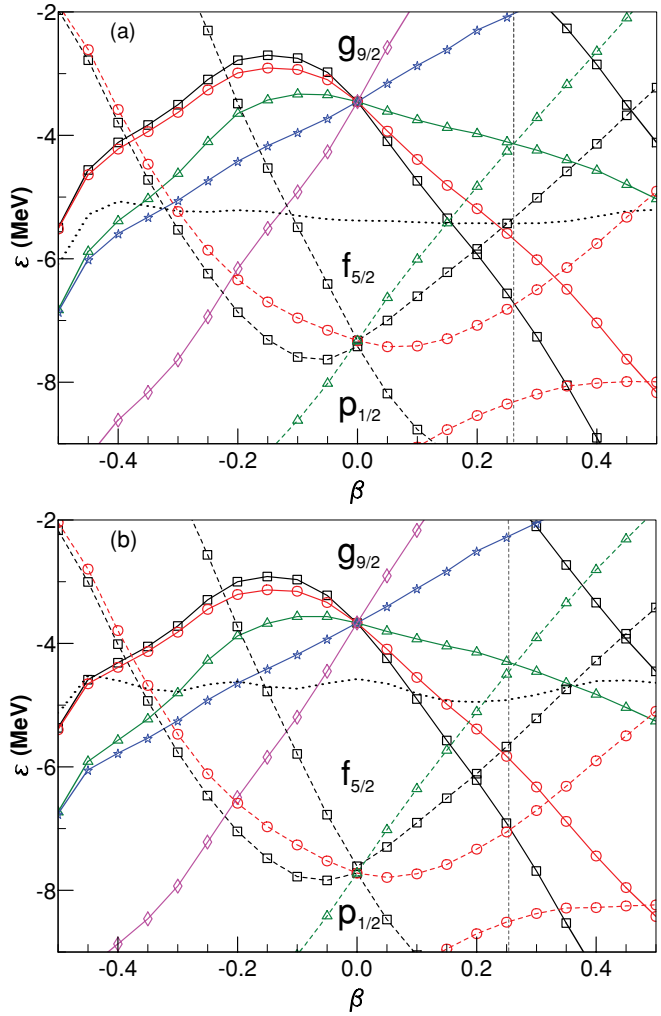

FIG. 9. (Color online) Neutron single-particle levels from axial HFB calculations for (a) ^{66}Fe and (b) ^{68}Fe. Dotted lines are for Fermi energies. Vertical dashed lines drawn at deformations $\beta = 0.261$ (^{66}Fe) and $\beta = 0.254$ (^{68}Fe) indicate levels of present interest for ^{67}Fe spectrum analysis (see text). Dashed (solid) lines represent negative (positive) parity K^π states. Squares are for $K = 1/2$, circles are for $K = 3/2$, triangles are for $K = 5/2$, stars are for $K = 7/2$, and diamonds are for $K = 9/2$. Single-particle energies are in MeV.

Both calculated bands shown in Fig. 10 display similar features.

Assigning the $5/2^-$ band member at either 366.4- or 387.7-keV excitation energy, two γ rays are expected to depopulate this level: one feeding the $1/2^-$ state and the other feeding the $3/2^-$ level. In this scenario, the $E2$ reduced probabilities for the $5/2^- \rightarrow 1/2^-$ and $5/2^- \rightarrow 3/2^-$ collective transitions are estimated to be in the ratio 7/2 [61]. Combined with the expected value taken by the reduced $M1$ transition probability, the $5/2^- \rightarrow 3/2^-$ transition strength turns out to be approximately 10 times stronger than that for the $E2$ $5/2^- \rightarrow 1/2^-$ transition. As only one γ ray depopulating the $5/2^-$ collective state is observed, it is also possible that the $1/2^-$ and $3/2^-$ levels are actually almost degenerated in energy. With the energy resolution of our setup, this means

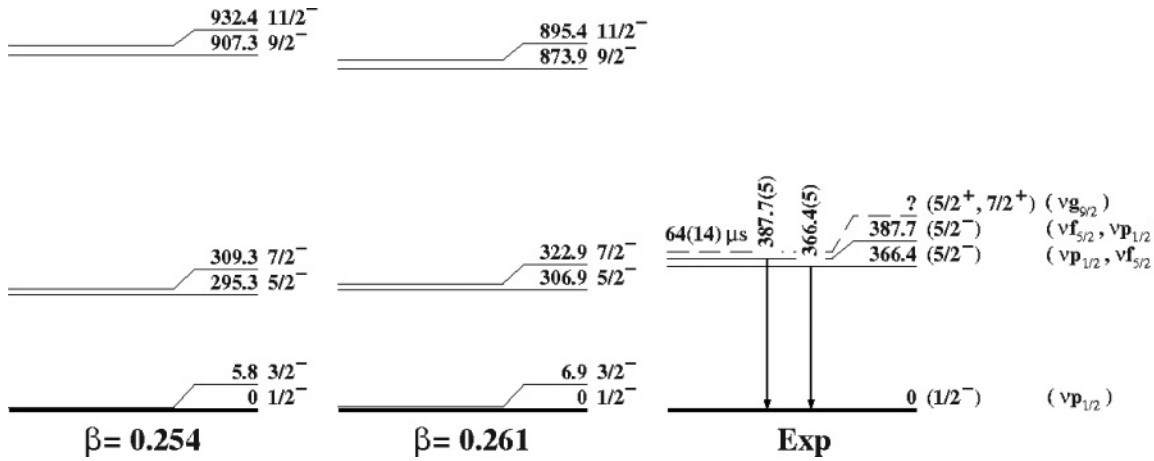

FIG. 10. ^{67}Fe level scheme. (left, middle) Decoupled rotational band calculated at the even-even core deformations $\langle\beta\rangle = 0.261$ (^{66}Fe) and $\langle\beta\rangle = 0.254$ (^{68}Fe). (right) Experimental level scheme from present model studies as well as single-particle parentage assignments. For more details, see the text.

that the difference in transition energies should be $|\Delta E_\gamma| < 1$ keV [40,41]. As a summary of these discussions, we suggest that one of the $5/2^-$ levels is a collective excitation and/or that the low-lying $1/2^-$ and $3/2^-$ levels are degenerate in energy.

Assuming again that the $\beta(^{67}\text{Fe})$ deformation is that of the even cores, a $K^\pi = 5/2^-$ level originating from the $\nu f_{5/2}$ orbital is expected to show up in the level scheme. This excited state is expected to decay toward the $1/2^-$ and $3/2^-$ low-lying levels via weak $E2$ transitions. Furthermore, its $M1$ decay to the $3/2^-$ state is forbidden, as changes in orbital angular momentum l and K values are $2\hbar$ each ($\Delta l = 2$, $\Delta K = 2$), resulting in a hindrance factor equal to 4. The only decay processes available to this $5/2^-$ single-particle level are weak $E2$ transitions to $1/2^-$ and/or $3/2^-$ low-lying states. Only one $E2$ transition would then be observed if the $1/2^-$ and $3/2^-$ levels were degenerate in energy.

All these discussions based on the assumption that ^{67}Fe displays the same deformation as that of the cores lead to model predictions (hereafter called scenario I) that sound plausible as long as the low-lying levels actually are degenerate in energy, consistent with the $(1/2^-)$ ground-state spin and parity assignments [30].

2. *Rotation-alignment scheme*

An alternative to the above model assumption has been sought since the polarization effect of the neutron on the even-even core has so far been ignored. This effect could be strong since the core, either ^{66}Fe or ^{68}Fe, is soft against deformation. Treating such an effect forms the next step in our model analysis. Guided by the previous model predictions in which the $K^\pi = 5/2^-$ level of $\nu f_{5/2}$ parentage had an excitation energy as high as $E_x = 1.2$ MeV, we have considered deformations in the single-particle level scheme in Fig. 9 that would provide a lower excitation energy for this state. We have found that $\beta \approx 0.2$ would be suitable for this purpose. An immediate consequence of considering lower deformation than previously assumed is that the picture of decoupled rotational bands is no longer appropriate. Instead, we will consider that rotation alignment is the picture [62] that deserves consideration. With $\beta = 0.2$ as quadrupole deformation, the condition $|\beta A^{2/3}| < 4$ for using the weak-coupling scheme is fulfilled for ^{67}Fe [63].

At the $\beta = 0.2$ quadrupole deformation, the Nilsson diagram in Fig. 9 suggests that the ground state is a $K^\pi = 3/2^+$ level of $\nu g_{9/2}$ parentage with a few hundred keV difference between this level and the $K^\pi = 1/2^-$ level of $\nu p_{1/2}$ parentage. Assuming that the spherical $N = 40$ gap in ^{67}Fe is slightly weaker than that calculated for the even-even cores, the $K^\pi = 3/2^+$ level drops below the $K^\pi = 1/2^-$ state. As a consequence, we suggest that the spin and parity of the ground state might still be $K^\pi = 1/2^-$. The $K^\pi = 5/2^-$ level originating from the $\nu f_{5/2}$ orbital takes on the excitation energy $E_x \approx 500$ keV. The prolate decoupled band built on top of the $I^\pi = K^\pi = 1/2^-$ ground state is expected to display stretched $E2$ transitions, and it includes a $I^\pi = 5/2^-$ state as a band member. If the even-core ^{66}Fe were rigid, this collective level would be located at $E_x = 574$ keV, which is the measured 2_1^+ excitation energy. None of the observed excitation energies for the $5/2^-$ levels ($E_x \approx 400$ keV) are close to $E_x = 574$ keV for this 2_1^+ level, suggesting that the assumptions underlying the rotation-alignment model are not strictly fulfilled. However, the rotation-alignment picture provides a qualitative interpretation of the observed spectrum: only one $E2$ collective transition takes place between either one of the $5/2^-$ levels and the $1/2^-$ ground state. The other observed γ ray arises from the $\nu f_{5/2} \rightarrow \nu p_{1/2}$ noncollective $E2$ transition. Consistent with the above model assumption (i.e., reduction of the spherical $N = 40$ gap), the $K^\pi = 5/2^+$ state becomes a candidate for the isomeric state lying above the $K^\pi = 5/2^-$ state.

As the even-even cores are soft against deformation, it seems that the rotation-alignment scheme provides a sound interpretation of present and previous γ-ray decay measurements. $I^\pi = 1/2^-$ is therefore inferred for spin and parity assignments to the ^{67}Fe ground state. This interpretation (called scenario II) will remain tentative until the g factor is measured for the ground state.

3. *Proposed level scheme*

The $I^\pi = 5/2^+$ or $7/2^+$, 64-μs isomer of $\nu g_{9/2}$ parentage may take place either at deformation close to that for the gs or at oblate deformation $\beta \approx -0.2$. Its excitation energy has not been determined, but an estimate could be suggested. For a nonobserved transition below 30 keV, the energy limitation of our setup, only $E1$ transitions to $5/2^-$ levels lead to half-lives compatible with that measured. An $M2$ (or $E3$) branch from a $5/2^+$ isomer to the $1/2^-$ ground state will be suppressed by the l forbiddance of such an intrinsically $\nu g_{9/2} \rightarrow \nu p_{1/2}$ transition. There is a no reason to exclude either $I^\pi = 5/2^+$ or $I^\pi = 7/2^+$ for the spin and parity assignments to the isomeric level.

The right panel of Fig. 10 shows the proposed experimental level scheme together with the present orbital parentage assignments. Our interpretation of the ^{67}Fe low excitation energy spectrum will retain a tentative character until the γ degree of freedom of the even cores is considered in extended model calculations.

V. CONCLUSION

Systematic measurements of β-decay properties have been performed at GANIL for 29 neutron-rich nuclei from Ti to Co, with masses in the range $A = 58$–74. Half-lives have been determined, among which those for ^{61}Ti, ^{64}V, and ^{71}Fe are new. Conventional structure model calculations in which axial quadrupole deformations are assumed provide half-life values that, in general, do not match the present data. This experiment has also provided information on prompt β-delayed γ-ray spectroscopy of the ^{67,68}Mn measurements that have been challenged with microscopic structure model predictions. These latter measurements provide γ-ray transitions in the ^{67}Fe daughter nucleus, from which it is inferred that the known isomeric state lies higher in energy than previously estimated. The $2^+ \rightarrow 0^+$ transition in ^{66}Fe was also observed, which allowed us to provide a 10(5)% lower limit for the ^{67}Mn β-delayed neutron probability. Prompt γ-ray transitions were observed in ^{68}Fe, from which high-precision excitation energies for the yrast (2^+) and (4^+) states are reported, matching those from previous γ-ray spectroscopy measurements. Those γ rays were observed with similar intensities, suggesting a ground-state spin $I > 3$ for the ^{68}Mn.

Spins and parities were tentatively assigned to the ^{67}Fe levels on the basis of separate measurements and systematics. A first tentative interpretation of the data was based on axial HFB calculations with the D1S force that treated this even-odd nucleus using the blocking method (scenario I). Assuming that the quadrupole deformation is the same as that calculated for the even-even ^{66}Fe and ^{68}Fe cores, the mean-field calculations support the $K^\pi = 1/2^-$ assignments for the ground state that originates from the $\nu p_{1/2}$ orbital with mean deformation $\beta \approx 0.26$. Our interpretation points to a possible degeneracy in energy of the $I^\pi = 1/2^-$ and $I^\pi = 3/2^-$ levels. One of the two observed excited states is proposed to be the $I^\pi = 5/2^-$ member of the ground-state decoupled band, while the other is of single-particle character with $\nu f_{5/2}$ parentage. In scenario II, we have left out the previous assumption that the even core of ^{67}Fe is not polarized by adding one neutron. Our interpretation of the γ-ray transitions is based on the rotation-alignment picture where the assumed quadrupole deformation $\beta = +0.2$ is weaker than $\beta = +0.26$ in scenario I. Results are as follows: (i) the ground state of $\nu p_{1/2}$ parentage is assigned $I^\pi = 1/2^-$, (ii) one of the observed excited states decays to the $I^\pi = 1/2^-$ level by a collective $E2$ transition, and (iii) the other observed excited state is $I^\pi = 5/2^-$ of $\nu f_{5/2}$ parentage, which decays to the ground state via a noncollective $E2$ transition. In both scenarios, the isomeric state is interpreted as originating from the $\nu g_{9/2}$ orbital, with $I^\pi = 5/2^+$ or $7/2^+$. We think that scenario II is more appropriate for interpreting the low-energy level scheme and related γ-ray decay properties. Experimental information such as g-factor measurements for ground and isomeric states and Coulomb excitation measurements would be valuable assets for supporting the rotation-alignment picture.

More detailed discussions on the $N = 41$ Fe isotope structure imply that axial symmetry should be released in the HFB calculations. This statement is of broad relevance as it addresses the major issue of extending beyond-mean-field methods to all even-odd nuclei. This task will be particularly challenging for odd-A nuclei with even-even cores soft against axial and triaxial deformations, features typical of ^{66}Fe and ^{68}Fe.

In even-even Fe isotopes, the observed yrast 2^+ level smoothly drops in excitation energy with N increasing from $N = 36$ to $N = 42$, a feature well reproduced by the present beyond-mean-field calculations based on the D1S effective force. It is expected that the 2^+ excitation energy will further decrease for higher-mass Fe isotopes and will reach a plateau approximately two neutrons below the $N = 50$ shell closure. The picture stemming from the present calculations is that of deformed nuclei prone to stretch with growing angular momentum, thus making the structure indicator R_{42} in this mass region of little pertinence. The neutron-rich Fe isotopes may be considered as soft rotors, a conclusion similar to that provided in Ref. [17]. As the development of soft deformation in this mass region is mainly rooted to increasing occupation number of the $g_{9/2}$ and $d_{5/2}$ neutron orbitals, it would be most interesting to extend experimental spectroscopic studies to larger neutron excess for both iron and chromium elements. Such studies will offer an opportunity for further challenging the D1S force properties far from stability. Finally, the present β-decay half-life measurements form a database that would be worth consideration in a new generation of QRPA calculations involving more realistic deformations than assumed in previous works. In this respect, handling triaxial nuclear shapes seems to be a key issue in the present mass region.

ACKNOWLEDGMENTS

We are grateful for the technical support provided by the staff of the GANIL facility. This work has been partially supported by the EU Access to Large Scale Facilities Program. The germanium detectors used in this experiment were provided by the EXOGAM collaboration. ORNL is managed

by UT-Battelle, LLC, for the U.S. Department of Energy under Contract No. DE-AC05-00OR22725. One of us (A.B.) acknowledges the partial financial support from CNCSIS, Romania, under Grant IDEI No. 294/2007.

[1] J. Dobaczewski, I. Hamamoto, W. Nazarewicz, and J. A. Sheikh, Phys. Rev. Lett. **72**, 981 (1994).
[2] H. Grawe, Acta Phys. Pol. B **34**, 2267 (2003); H. Grawe, K. Langanke, and G. Martinez-Pinedo, Rep. Prog. Phys. **70**, 1525 (2007).
[3] T. Otsuka, T. Suzuki, M. Honma, Y. Utsuno, N. Tsunoda, K. Tsukiyama, and M. Hjorth-Jensen, Phys. Rev. Lett. **104**, 012501 (2010), and references therein.
[4] M. Girod, Ph. Dessagne, M. Bernas, M. Langevin, F. Pougheon, and P. Roussel, Phys. Rev. C **37**, 2600 (1988).
[5] A. M. Oros-Peusquens and P. F. Mantica, Nucl. Phys. A **669**, 81 (2000).
[6] K. H. Langanke, J. Terasaki, F. Nowacki, D. J. Dean, and W. Nazarewicz, Phys. Rev. C **67**, 044314 (2003).
[7] L. Gaudefroy, A. Obertelli, S. Peru, N. Pillet, S. Hilaire, J.-P. Delaroche, M. Girod, and J. Libert, Phys. Rev. C **80**, 064313 (2009).
[8] R. Broda *et al.*, Phys. Rev. Lett. **74**, 868 (1995).
[9] M. Hannawald *et al.*, Phys. Rev. Lett. **82**, 1391 (1999).
[10] S. Leenhardt *et al.*, Eur. Phys. J. A **14**, 1 (2002).
[11] O. Sorlin *et al.*, Phys. Rev. Lett. **88**, 092501 (2002).
[12] C. Guénaut *et al.*, Eur. Phys. J. A **25**, Suppl. **1**, 33 (2005).
[13] N. Aoi *et al.*, Phys. Rev. Lett. **102**, 012502 (2009).
[14] M. Bernas, Ph. Dessagne, M. Langevin, G. Parrot, F. Pougheon, E. Quiniou, and P. Roussel, J. Phys. Lett. **45**, 851 (1984).
[15] R. Grzywacz *et al.*, Phys. Rev. Lett. **81**, 766 (1998).
[16] P. Möller, J. R. Nix, and K.-L. Kratz, At. Data Nucl. Data Tables **66**, 131 (1997).
[17] Y. Sun, Y. C. Yang, H. L. Liu, K. Kaneko, M. Hasegawa, and T. Mizusaki, Phys. Rev. C **80**, 054306 (2009).
[18] J. Dechargé and D. Gogny, Phys. Rev. C **21**, 1568 (1980); J. F. Berger, M. Girod, and D. Gogny, Comput. Phys. Commun. **63**, 385 (1991).
[19] R. Anne, in *Proceedings of the International Symposium on Exotic Nuclei 2001*, edited by Yu. E. Penionzhkevich and E. A. Cherepanov (World Scientific, Singapore, 2001), p. 634.
[20] S. Rab, Nucl. Data Sheets **63**, 1 (1991).
[21] D. Bazin, D. Guerreau, R. Anne, D. Guillemaud-Mueller, A. C. Mueller, and M. G. Saint-Laurent, Nucl. Phys. A **515**, 349 (1990).
[22] L. Gaudefroy *et al.*, Eur. Phys. J. A **23**, 41 (2005).
[23] I. N. Borzov, Phys. Rev. C **71**, 065801 (2005).
[24] P. Hosmer *et al.*, Phys. Rev. C **82**, 025806 (2010).
[25] M. Sawicka *et al.*, Phys. Rev. C **68**, 044304 (2003).
[26] M. Sawicka *et al.*, Eur. Phys. J. A **22**, 455 (2004).
[27] O. Sorlin *et al.*, Nucl. Phys. A **719**, 193c (2003).
[28] O. Sorlin *et al.*, Nucl. Phys. A **660**, 3 (1999); **669**, 351(E) (2000).
[29] O. Sorlin *et al.*, Eur. Phys. J. A **16**, 55 (2003).
[30] D. Pauwels *et al.*, Phys. Rev. C **79**, 044309 (2009).
[31] M. Bernas, P. Armbruster, S. Czajkowski, H. Faust, J. P. Bocquet, and R. Brissot, Phys. Rev. Lett. **67**, 3661 (1991).
[32] W. F. Mueller *et al.*, Phys. Rev. Lett. **83**, 3613 (1999).
[33] W. F. Mueller *et al.*, Phys. Rev. C **61**, 054308 (2000).
[34] C. Mazzocchi *et al.*, Phys. Lett. B **622**, 45 (2005).
[35] F. Ameil *et al.*, Eur. Phys. J. A **1**, 275 (1998).
[36] S. Franchoo *et al.*, Phys. Rev. Lett. **81**, 3100 (1998).
[37] P. Möller, J. R. Nix, W. D. Myers, and J. Swiatecki, At. Data Nucl. Data Tables **59**, 185 (1995).
[38] Y. Aboussir, J. M. Pearson, A. K. Dutta, and F. Tondeur, At. Data Nucl. Data Tables **61**, 127 (1995).
[39] J. Pereira *et al.*, Phys. Rev. C **79**, 035806 (2009), and references therein.
[40] M. Sawicka *et al.*, Eur. Phys. J. A **16**, 51 (2003).
[41] J. M. Daugas *et al.*, AIP Conf. Proc. **831**, 427 (2006).
[42] M. Block *et al.*, Phys. Rev. Lett. **100**, 132501 (2008).
[43] P. Adrich *et al.*, Phys. Rev. C **77**, 054306 (2008).
[44] J. Libert, M. Girod, and J. P. Delaroche, Phys. Rev. C **60**, 054301 (1999), and references therein.
[45] J. P. Delaroche, M. Girod, J. Libert, H. Goutte, S. Hilaire, S. Péru, N. Pillet, and G. F. Bertsch, Phys. Rev. C **81**, 014303 (2010), and references therein.
[46] D. J. Thouless and J. G. Valatin, Nucl. Phys. A **31**, 211 (1962).
[47] K. Kumar and M. Baranger, Nucl. Phys. A **92**, 608 (1967).
[48] S. Goriely, S. Hilaire, M. Girod, and S. Péru, Phys. Lett. **102**, 242501 (2009).
[49] L. Grodzins, Phys. Lett. **2**, 88 (1962).
[50] R. Rodrìguez-Guzmàn, P. Sarriguren, L. M. Robledo, and J. E. Garcìa-Ramos, Phys. Rev. C **81**, 024310 (2010).
[51] E. Caurier, F. Nowacki, and A. Poves, Eur. Phys. J. A **15**, 145 (2002).
[52] M. Honma, T. Otsuka, B. A. Brown, and T. Mizusaki, Phys. Rev. C **69**, 034335 (2004).
[53] M. C. East, A. E. Stuchbery, S. K. Chamoli, J. S. Pinter, H. L. Crawford, A. N. Wilson, T. Kibedi, and P. F. Mantica, Phys. Rev. C **79**, 024304 (2009).
[54] M. Honma, T. Otsuka, T. Mizusaki, and M. Hjorth-Jensen, Phys. Rev. C **80**, 064323 (2009).
[55] H. Oba, M. Matsuo, Prog. Theor. Phys. **120**, 143 (2008).
[56] C. Özen, K. Langanke, G. Martinez-Pinedo, and D. J. Dean, Phys. Rev. C **75**, 064307 (2007).
[57] J. Ljungvall *et al.*, Phys. Rev. C **81**, 061301(R) (2010).
[58] K. Sieja and F. Nowacki, Phys. Rev. C **81**, 061303(R) (2010).
[59] D. R. Inglis, Phys. Rev. **103**, 1786 (1956).
[60] S. T. Belyaev, Nucl. Phys. A **24**, 322 (1961).
[61] A. Bohr and B. R. Mottelson, *Nuclear Structure*, Vol. 2 (Benjamin, Reading, MA, 1975).
[62] F. S. Stephens, Rev. Mod. Phys. **47**, 43 (1975).
[63] J. Meyer-Ter-Vehn, Nucl. Phys. A **249**, 111 (1975).